

Lorentz- and CPT-violating models for neutrino oscillations

Jorge S. Díaz and V. Alan Kostelecký

Physics Department, Indiana University, Bloomington, IN 47405, U.S.A.

(Dated: IUHET 561, August 2011)

A class of calculable global models for neutrino oscillations based on Lorentz and CPT violation is presented. One simple example matches established neutrino data from accelerator, atmospheric, reactor, and solar experiments, using only two degrees of freedom instead of the usual five. A third degree of freedom appears in the model, and it naturally generates the MiniBooNE low-energy anomalies. More involved models in this class can also accommodate the LSND anomaly and neutrino-antineutrino differences of the MINOS type. The models predict some striking signals in various ongoing and future experiments.

I. INTRODUCTION

The minimal Standard Model (SM) of particle physics contains three flavors of massless left-handed neutrinos. However, experiments with solar, reactor, accelerator, and atmospheric neutrinos have convincingly demonstrated the existence of neutrino flavor oscillations. This effect cannot be accommodated within the SM and so represents forceful evidence for new physics.

A popular hypothesis attributes neutrino oscillations to the existence of a tiny neutrino mass matrix with off-diagonal components. Extending the SM to incorporate this notion produces a model with three flavors of massive neutrinos (3ν SM), in which oscillations are controlled by a 3×3 matrix involving six parameters: two mass-squared differences Δm_{\odot}^2 , Δm_{atm}^2 , three angles θ_{12} , θ_{23} , θ_{13} , and a phase δ controlling CP violation. The first four of these parameters must be nonzero to match established experimental data, while recent results provide indications that the angle θ_{13} must also be nonzero [1, 2].

In this work, we explore an alternative hypothesis attributing part of the observed neutrino oscillations to tiny Lorentz and CPT violation, which might arise in a Planck-scale theory unifying gravity and quantum physics such as string theory [3]. One motivation for studying alternative hypotheses for neutrino oscillations is based on existing data. Several neutrino experiments have reported potential evidence for anomalous neutrino oscillations that is incompatible with the 3ν SM. This includes the LSND signal [4], the MiniBooNE low-energy excess [5], and neutrino-antineutrino differences in the MiniBooNE [6] and MINOS [7] experiments. Another motivation is philosophical: having more than one viable hypothesis is known to be of great value in guiding experimental and theoretical investigations of new physics. Lorentz and CPT violation is interesting in this context because it naturally generates neutrino oscillations and moreover leads to simple global models describing all established and anomalous neutrino data [8, 9].

An appropriate theoretical framework for studying realistic signals of Lorentz violation is effective field theory [10]. In this context, CPT violation is necessarily accompanied by Lorentz violation [11], and the comprehensive description for Lorentz and CPT violation

containing the SM and General Relativity is given by the Standard-Model Extension (SME) [12, 13]. In the SME action, each Lorentz-violating term is a coordinate-independent quantity constructed from the product of a Lorentz-violating operator and a controlling coefficient. The combination of observer coordinate invariance and Lorentz violation implies particles in the SME follow trajectories in a pseudo-Riemann-Finsler geometry [14].

Over the last decade or so, many experimental analyses using a broad variety of techniques have been performed to seek nonzero SME coefficients for Lorentz and CPT violation [15]. The interferometric nature of particle oscillations suggests that sensitive neutrino or neutral-meson experiments might well yield the first detectable signals of tiny Lorentz violation. In the neutrino sector, recent SME-based phenomenological studies [8, 9, 16–33] and methodologies for experimental analysis [34, 35] have spurred searches for Lorentz and CPT violation by the LSND [36], Super-Kamiokande (SK) [37], MINOS [38, 39], MiniBooNE [40], and IceCube collaborations [41]. Searches have also been performed with neutral mesons [42, 43], and recent D0 results suggest some evidence for anomalous CP violation [44] that could be attributed to Lorentz and CPT violation [45].

Here, we focus on a special class of ‘puma’ models in which the 3×3 effective hamiltonian h_{eff}^{ν} governing oscillations of three flavors of active left-handed neutrinos is characterized by two simple properties: isotropic Lorentz violation, and a zero eigenvalue [9]. The isotropic Lorentz violation implies boost invariance is broken while leaving rotations unaffected, so h_{eff}^{ν} is independent of the direction of the neutrino momentum but must contain unconventional dependence on the neutrino energy E . This leads to unconventional energy dependences even in vacuum oscillations, producing a broad range of unique neutrino behavior. The zero eigenvalue can be attributed to a discrete symmetry of h_{eff}^{ν} . It ensures quadratic calculability of the mixing matrix and of oscillation probabilities for all models, even when matter effects are included. These two features differ qualitatively from the 3ν SM, in which the Lorentz-invariant mass terms force a $1/E$ energy dependence of all terms in h_{eff}^{ν} and the lack of symmetry results in calculational complexity.

The unconventional energy dependence in h_{eff}^{ν} generically takes the form of polynomials in E arising from

Lorentz-violating operators of arbitrary dimension in the SME Lagrange density [46]. The polynomial coefficients are therefore determined in terms of SME coefficients for Lorentz violation. For much of this work we make the plausible assumption that a few terms of comparatively low mass dimension dominate the neutrino behavior, either by chance or due to the presently unknown structure of the underlying theory, and hence that only a few coefficients are needed to reproduce the bulk of existing neutrino data. Indeed, the basic puma models considered below have only three degrees of freedom, which includes one mass and two Lorentz-violating coefficients. Remarkably, two of these degrees of freedom suffice to reproduce all established neutrino behavior, a frugal result compared to the five degrees of freedom required by the 3ν SM. Moreover, the third degree of freedom naturally reproduces the anomalous results found by MiniBooNE [5, 6] without introducing new particles or forces. Comparatively minor modifications of these simple puma models that preserve the discrete symmetry of h_{eff}^ν can also accommodate the LSND signal [4] and anomalies of the MINOS type [7].

The structure of this paper is as follows. The basic properties of the general puma models are presented in Sec. II. Applications to existing experiments are discussed in Sec. III. A specific model involving one mass parameter and two Lorentz-violating operators, one of which is CPT odd, is used for illustrative purposes. Predictions for future experiments are presented in Sec. IV. Some of these are strikingly different from models based on the 3ν SM. Variant puma models using three different degrees of freedom or more than three parameters are considered in Sec. V. Finally, Sec. VI contains some comments on the general nature of the models.

The notation adopted here is that of Refs. [8, 9]. A mass parameter is denoted m , a coefficient for isotropic CPT-odd Lorentz violation is denoted $\hat{a}^{(d)}$, and a coefficient for isotropic CPT-even Lorentz violation is denoted $\hat{c}^{(d)}$, where d is the dimension of the corresponding operator. To identify the various specific puma models according to their coefficient content, we introduce a convenient nomenclature listing coefficients in descending order of operator mass dimension. For example, a model with three degrees of freedom including a mass term m and coefficients $\hat{a}^{(5)}$ and $\hat{c}^{(8)}$ for Lorentz violation is called a $c_8 a_5 m$ model.

II. GENERAL MODEL

In the general puma model, the effective 3×3 hamiltonian h_{eff}^ν describing the oscillation of three active neutrino flavors e, μ, τ takes the form [9]

$$h_{\text{eff}}^\nu = A \begin{pmatrix} 1 & 1 & 1 \\ 1 & 1 & 1 \\ 1 & 1 & 1 \end{pmatrix} + B \begin{pmatrix} 1 & 1 & 1 \\ 1 & 0 & 0 \\ 1 & 0 & 0 \end{pmatrix} + C \begin{pmatrix} 1 & 0 & 0 \\ 0 & 0 & 0 \\ 0 & 0 & 0 \end{pmatrix}, \quad (1)$$

where $A(E)$, $B(E)$, and $C(E)$ are real functions of the neutrino energy E . In this work, the function A is chosen to be $A = m^2/2E$, where m is the unique neutrino mass parameter in the theory. The functions B and C have nonstandard energy dependence, which here is taken to arise from Lorentz-violating terms in the SME, some of which may lie in the nonrenormalizable sector. The treatment of possible contributions to h_{eff}^ν from Lorentz-invariant operators lies outside our present scope and will be given elsewhere. We assume all SME coefficients contributing to h_{eff}^ν are spacetime constants, so the model (1) incorporates translation invariance and conserves energy and momentum. In the context of spontaneous Lorentz violation, where the SME coefficients can be interpreted in terms of expectation values in an underlying theory, this assumption implies soliton solutions, massive modes, and Nambu-Goldstone modes [47] are disregarded. The latter may play the role of the graviton [48], the photon in Einstein-Maxwell theory [49], or various new forces [50]. For simplicity in most specific models considered here, B and C are taken to be monomials in E , although more complicated polynomials or nonpolynomial functions can also be of interest.

The function A decreases inversely with energy, while B and C typically increase. At low energies, the effective hamiltonian h_{eff}^ν is therefore well approximated by the A term alone. This term has a ‘democratic’ form, exhibiting symmetry under the permutation group S_3 acting on the three neutrino flavors e, μ, τ . In contrast, the nonstandard energy dependences in the B and C terms dominate at high energies. The flavor-space structure of these terms breaks the S_3 symmetry to its S_2 subgroup in the μ - τ sector.

For antineutrinos, oscillations are governed by the CPT image $h_{\text{eff}}^{\bar{\nu}}$ of the effective hamiltonian h_{eff}^ν . The effect of the CPT transformation on h_{eff}^ν is to change the signs of any coefficients for Lorentz violation that are associated with CPT-odd operators in the SME. Since mass terms are invariant under CPT [11], the A term in h_{eff}^ν is unaffected by the transformation. At low energies, the full permutation symmetry of the puma model is therefore $S_3 \times \bar{S}_3$, where \bar{S}_3 is the symmetry acting on antineutrino flavors. At high energies, the $S_3 \times \bar{S}_3$ invariance breaks to $S_2 \times \bar{S}_2$. If any coefficients for CPT-odd Lorentz violation are present, differences between neutrinos and antineutrinos can become manifest.

An elegant feature of the puma model is the existence of a zero eigenvalue for the effective hamiltonian, which is a consequence of the permutation symmetry of the texture (1). This implies considerable calculational simplification compared to the 3ν SM and typical other neutrino-oscillation models. Many results can be obtained exactly by hand even when all three neutrino flavors mix. A short calculation reveals that the eigenvalues $\lambda_{a'}$, $a' = 1, 2, 3$,

of the effective hamiltonian h_{eff}^ν take the exact form

$$\begin{aligned}\lambda_1 &= \frac{1}{2} \left[3A + B + C - \sqrt{(A - B - C)^2 + 8(A + B)^2} \right], \\ \lambda_2 &= \frac{1}{2} \left[3A + B + C + \sqrt{(A - B - C)^2 + 8(A + B)^2} \right], \\ \lambda_3 &= 0.\end{aligned}\quad (2)$$

The mixing matrix $U_{a'a}$ that diagonalizes h_{eff}^ν can also be expressed exactly as

$$U_{a'a} = \begin{pmatrix} \frac{\lambda_1 - 2A}{N_1} & \frac{A+B}{N_1} & \frac{A+B}{N_1} \\ \frac{\lambda_2 - 2A}{N_2} & \frac{A+B}{N_2} & \frac{A+B}{N_2} \\ 0 & -\frac{1}{\sqrt{2}} & \frac{1}{\sqrt{2}} \end{pmatrix}.\quad (3)$$

In this equation, the index a ranges over $a = e, \mu, \tau$ and the normalization factors are

$$\begin{aligned}N_1 &= \sqrt{(\lambda_1 - 2A)^2 + 2(A + B)^2}, \\ N_2 &= \sqrt{(\lambda_2 - 2A)^2 + 2(A + B)^2}.\end{aligned}\quad (4)$$

The eigenvalues $\bar{\lambda}_{a'}$, the mixing matrix $\bar{U}_{a'a}$, and the normalization factors \bar{N}_1, \bar{N}_2 for the antineutrino effective hamiltonian $h_{\text{eff}}^{\bar{\nu}}$ are obtained by CPT conjugation of B and C .

In the low-energy limit, the mixing matrix (3) reduces to the tribimaximal form originally postulated on phenomenological grounds by Harrison, Perkins, and Scott [51]. The democratic structure of the A term in h_{eff}^ν therefore ensures tribimaximal mixing of the three neutrino flavors at low energies. Combined with the choice $A = m^2/2E > 0$, this mixing guarantees agreement of the puma model with low-energy solar neutrinos [52] and with the mixing observed in KamLAND [53]. For a suitable choice of mass parameter m , as discussed in the next section, the A term can also correctly describe the L/E oscillation signature observed by KamLAND [54].

Another defining feature of the puma model is a Lorentz-violating seesaw [8] that mimics a mass term at high energies, without invoking mass. This differs from the usual seesaw mechanism [55, 56], which is based on mass terms in the action. Suppose B and C are monomials of the form

$$B(E) = \dot{k}^{(p)} E^{p-3}, \quad C(E) = \dot{c}^{(q)} E^{q-3}, \quad (5)$$

where p and q are the dimensions of the operators associated with the coefficients $\dot{k}^{(p)}$ and $\dot{c}^{(q)}$. In this work, we take $\dot{c}^{(q)} > 0$ for definiteness but consider both sign options for $\dot{k}^{(p)}$. Reversing the sign of $\dot{c}^{(q)}$ produces phenomenology closely related to reversing instead the sign of $\dot{k}^{(p)}$, as can be seen by inspecting Eqs. (2) and (3). If $q > p$ then C grows faster than B , so at high energies

$$\lambda_1 \approx -\frac{2B^2}{C} = -\frac{2(\dot{k}^{(p)})^2 E^{2p-q-3}}{\dot{c}^{(q)}}.\quad (6)$$

For the choice $q = 2(p - 1)$, the eigenvalue λ_1 is proportional to $1/E$ and therefore plays the role of an effective mass term, even though no mass parameter is present at high energies. Note that imposing this choice requires the dominant coefficient in C to be CPT even. The null entries in the μ - τ block of h_{eff}^ν and the fast-growing ee element guarantee maximal $\nu_\mu \leftrightarrow \nu_\tau$ mixing at high energies, consistent with observations of atmospheric neutrinos [57–59]. For a suitable choice of the ratio B^2/C , as discussed in the next section, the seesaw mechanism also reproduces the L/E oscillation signature in the SK experiment [60].

Since the elements of h_{eff}^ν are real, the probability $P_{\nu_b \rightarrow \nu_a}$ of oscillation from ν_b to ν_a can be written in the simple form

$$P_{\nu_b \rightarrow \nu_a} = \delta_{ab} - 4 \sum_{a' > b'} U_{a'a} U_{a'b} U_{b'a} U_{b'b} \sin^2(\Delta_{a'b'} L/2), \quad (7)$$

where the quantities $\Delta_{a'b'} = \lambda_{a'} - \lambda_{b'}$ are the eigenvalue differences and L is the baseline. For each flavor pair a, b , the above sum contains three terms labeled by the values of $a', b' < a'$. Each term is the product of an amplitude $-4UUUU$ with a sinusoidal phase. The antineutrino-oscillation probabilities $P_{\bar{\nu}_b \rightarrow \bar{\nu}_a}$ are obtained by CPT conjugation. Since A, B , and C are real, all processes are T invariant. As a result, CP violation occurs if and only if CPT violation does. Notice that CP-violating effects can appear even though no analogue of the phase δ in the 3ν SM exists in the puma model.

All the above properties are insensitive to the ee component of the B term in h_{eff}^ν . As a result, a modified texture h_{eff}^ν can be constructed in which the ee entry in the B term vanishes. We have verified that most of the properties discussed in the remainder of this work remain unchanged for this modified texture. One exception is the renormalizable model presented in Sec. V A, for which we use a zero ee entry in the B term because the nonzero value produces a tension between the descriptions of long-baseline reactor and of solar neutrinos.

III. EXPERIMENTS

Next, we study the implications of the general model (1) for different experiments. Many characteristics of the model are generic. For definiteness, in this section we illustrate the discussion with a specific $c_8 a_5 m$ model [9]. Some comments on variant models are provided in Sec. IV.

The numerical values of the three parameters in the $c_8 a_5 m$ model are

$$\begin{aligned}m^2 &= 2.6 \times 10^{-23} \text{ GeV}^2, \\ \dot{a}^{(5)} &= -2.5 \times 10^{-19} \text{ GeV}^{-1}, \\ \dot{c}^{(8)} &= 1.0 \times 10^{-16} \text{ GeV}^{-4},\end{aligned}\quad (8)$$

The nonzero value of $\dot{a}^{(5)}$ implies this model contains CPT violation. The value for m^2 is consistent with limits

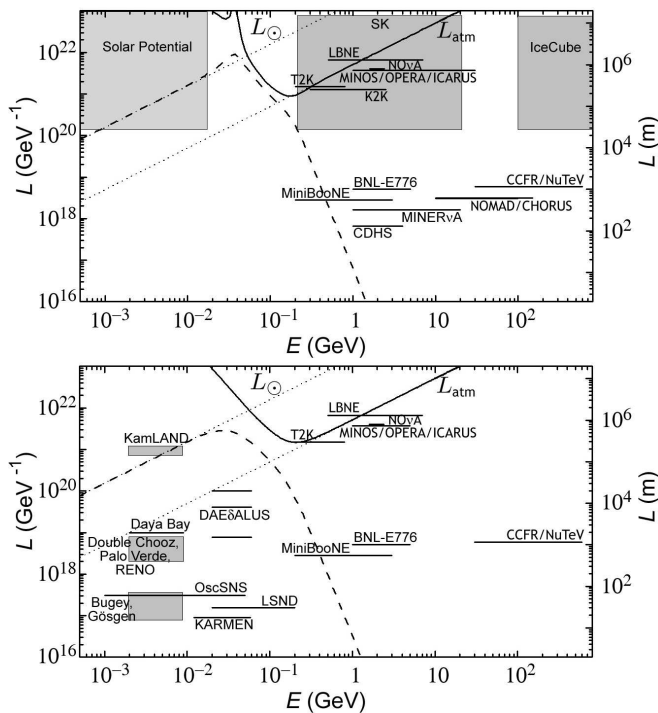


FIG. 1: Energy dependences of the oscillation lengths for neutrinos (top) and antineutrinos (bottom). The disappearance lengths for the puma model are L_{31} (top, solid line), L_{21} (top, dashed line), \bar{L}_{31} (bottom, solid line), and \bar{L}_{21} (bottom, dashed line), displayed for the values (8). The dotted lines are the disappearance lengths L_{\odot} (solar) and L_{atm} (atmospheric) in the $3\nu\text{SM}$.

from direct mass measurements and cosmological bounds [1].

By construction, $\hat{a}^{(5)}$ and $\hat{c}^{(8)}$ are the only nonzero SME coefficients defined in an isotropic frame I . In some scenarios, it is reasonable to identify I with a universal inertial frame U such as that defined by the cosmic microwave background (CMB), but other possibilities exist. Whatever the choice for I , the experiment frame E is boosted in it by some combination of the Earth's motion relative to the CMB, the Earth's revolution about the Sun, and the Earth's rotation. The coefficients $\hat{a}^{(5)}$ and $\hat{c}^{(8)}$ therefore induce anisotropic effects via the net boost in I . These could, for example, be detected by searches for sidereal or annual variations in E [42]. Experimental constraints and signals must be reported in a specified frame, but the frame E itself is inappropriate because it is noninertial and experiment specific. By convention, the canonical inertial frame used to report results is a Sun-centered frame S [15, 61]. Inspection reveals that the size of the effects in S induced by the values (8) all lie below the sensitivity levels achieved in experiments to date [36, 38–41]. Future experiments might offer improved sensitivity and thereby provide a distinct avenue for testing the model.

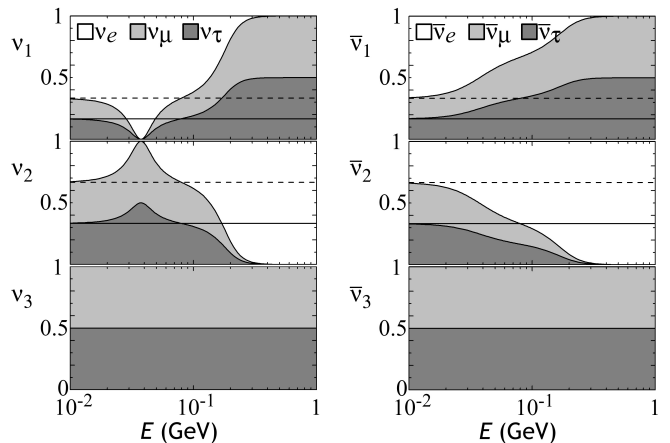


FIG. 2: Flavor content of the three neutrino eigenstates of h_{eff}^{ν} (left) and the three antineutrino eigenstates of $h_{\text{eff}}^{\bar{\nu}}$ (right) as a function of energy. For the puma model, the left-hand panel shows the energy dependences of $|U_{a'e}|^2$ (white), $|U_{a'\mu}|^2$ (light grey), and $|U_{a'\tau}|^2$ (dark grey) for each neutrino mass eigenstate $\nu_{a'}$, $a' = 1, 2, 3$, while the right-hand panel displays the analogous energy dependences for antineutrinos. For the $3\nu\text{SM}$, the corresponding quantities $|U_{a'e}|^2$ (regions above dashed lines), $|U_{a'\mu}|^2$ (regions between dashed and solid lines), and $|U_{a'\tau}|^2$ (regions below solid lines) for neutrinos and those for antineutrinos are energy independent. The models coincide at all energies for the eigenstates $\nu_3, \bar{\nu}_3$, but $\nu_1, \bar{\nu}_1$ match $\nu_2, \bar{\nu}_2$ only at low energies.

A. General features

The predictions of any model for neutrino and antineutrino oscillations can be visualized using a certain plot in E - L space [8]. Experiments are represented on the plot as regions determined by their baseline and energy coverage, while a given theory is represented by its characteristic oscillation wavelengths $L_{a'b'} = 2\pi/|\Delta_{a'b'}|$ associated with the eigenvalue differences $\Delta_{a'b'}(E)$. The absolute value is used because the oscillation phase is insensitive to the sign of $\Delta_{a'b'}$. Each curve $L_{a'b'} = L_{a'b'}(E)$ indicates the first maximum of a kinematic phase in the oscillation probability, thereby establishing the minimal distance from the neutrino source required for appearance or disappearance signals in a specific oscillation channel. Substantial signals appear in the region above each curve but are suppressed below it.

Figure 1 shows this plot for the puma model with values (8) and the $3\nu\text{SM}$. The $3\nu\text{SM}$ has two independent oscillation lengths, $L_{\odot} = 4\pi E/\Delta m_{\odot}^2$ and $L_{\text{atm}} = 4\pi E/\Delta m_{\text{atm}}^2$, both of which grow linearly with the energy and are therefore represented by straight lines in the plot. In the puma model, however, the unconventional energy dependences from $B(E)$ and $C(E)$ produce more general curves instead. These curves partially differ for neutrinos and antineutrinos, a consequence of the CPT violation implied by the values (8).

The figure shows that the puma curves merge with the 3ν SM lines L_\odot and L_{atm} at low and high energies, respectively, suggesting consistency of the puma model with results in KamLAND, solar, and atmospheric experiments. This agreement is confirmed in the subsections below. However, the two models are qualitatively different at intermediate energies.

Novel effects arise from the unconventional energy dependence of h_{eff}^ν , which generates energy-dependent mixing. The flavor content of the three eigenstates of h_{eff}^ν therefore changes with energy. Figure 2 shows this energy dependence for the values (8). At low energies, the flavor content approaches the tribimaximal limit. However, at high energies the eigenstate ν_2 becomes completely populated by ν_e . This implies the mixing $\nu_\mu \leftrightarrow \nu_\tau$ is maximal and controlled by Δ_{31} . The onset of this feature coincides with the onset of the Lorentz-violating seesaw. Indeed, as the mass term A becomes negligible in h_{eff}^ν , the fraction of ν_e in ν_2 grows with the separation between the lines L_{21} and L_{31} in Fig. 1.

Notice that the mixing angles in the 3ν SM are energy independent parameters that can freely be chosen to match data. In contrast, the mixing angles in the puma model at low and high energies are determined by the texture of h_{eff}^ν and therefore are fixed features of the model that cannot be adjusted according to experiment. This reduced freedom is one reason why the puma model offers a more economical description of confirmed neutrino data than the 3ν SM.

The energy dependence of the mixing matrix U implies the oscillation amplitudes $-4UUUU$ in each flavor channel and the corresponding probability (7) are also energy dependent. For given flavors a, b , the oscillation amplitudes are shown in Fig. 3. Note that negative amplitudes occur for disappearance channels, while positive amplitudes occur for appearance channels. The S_2 symmetry of h_{eff}^ν implies the four amplitudes for $\nu_e \rightarrow \nu_\tau$, $\bar{\nu}_e \rightarrow \bar{\nu}_\tau$, $\nu_\tau \rightarrow \nu_e$, and $\bar{\nu}_\tau \rightarrow \bar{\nu}_e$ are identical to those shown in the corresponding four central panels in the figure. The low-energy S_3 symmetry of h_{eff}^ν forces the low-energy amplitudes to values set by tribimaximal mixing and ensures the low-energy equalities $P_{\nu_e \rightarrow \nu_e} = P_{\nu_\mu \rightarrow \nu_\mu} = P_{\nu_\tau \rightarrow \nu_\tau}$ and $P_{\bar{\nu}_e \rightarrow \bar{\nu}_e} = P_{\bar{\nu}_\mu \rightarrow \bar{\nu}_\mu} = P_{\bar{\nu}_\tau \rightarrow \bar{\nu}_\tau}$. At high energies, the amplitudes become either zero or one due to the Lorentz-violating seesaw mechanism. The lower four panels in the figure reveal that the dominant amplitude at high energies has $(a', b') = (3, 1)$, leading to maximal $\nu_\mu \leftrightarrow \nu_\tau$ mixing and to an oscillation phase proportional to Δ_{31} and hence to $1/E$. Note also that the zero component U_{3e} of the mixing matrix (3), which is a consequence of the null eigenvalue of h_{eff}^ν , implies that the oscillation in any channel involving ν_e or $\bar{\nu}_e$ is controlled by only one amplitude because the other two vanish.

The three figures reveal many of the evolving properties associated with h_{eff}^ν and $h_{\text{eff}}^{\bar{\nu}}$ at intermediate energies. For example, a peak appears between 10 MeV and 100 MeV in the L_{31} curve for neutrinos in Fig. 1, accompanied by corresponding features in Figs. 2 and 3. The

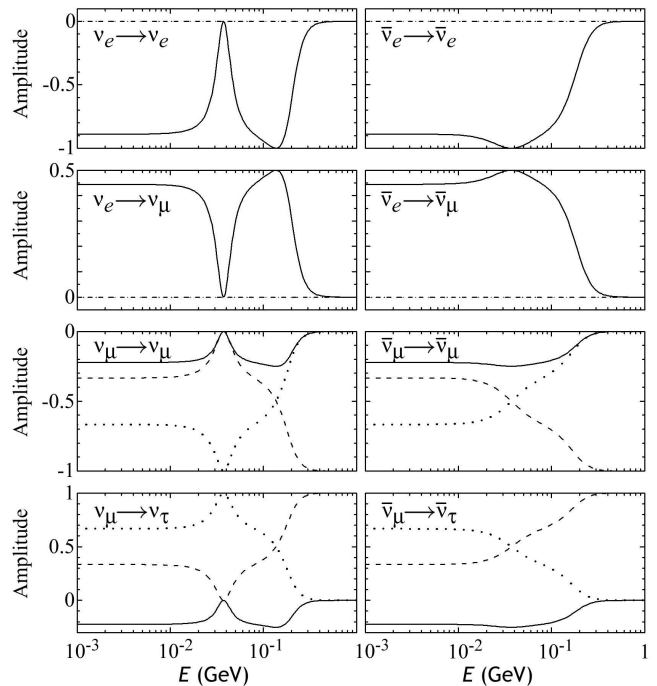


FIG. 3: Energy dependence of the oscillation amplitudes in the puma model. In each flavor channel, the amplitude factors $-4UUUU$ in Eq. (7) are plotted for each of the three (a', b') values 21 (solid lines), 31 (dashed lines), and 32 (dotted lines).

peak represents a divergence in L_{31} , which occurs when $\Delta_{a'b'}$ vanishes. Using the exact expressions (2) for the eigenvalues of h_{eff}^ν , we find that in general peaks occur for all positive energies E solving the equation

$$A(B - C) + B^2 = 0. \quad (9)$$

The peaks can in general occur for both neutrinos and antineutrinos. The absence of these features in the antineutrino plots suggests an origin in CPT violation. Since coefficients for CPT-odd Lorentz violation reverse sign under a CPT transformation, the nature of the solutions to Eq. (9) for antineutrinos changes. For the values (8), a single positive energy solves this equation for neutrinos, but no solutions exist for antineutrinos and hence no antineutrino peaks arise in Fig. 1.

B. Reactor antineutrinos

In the puma model, the general survival probability for reactor antineutrinos is

$$P_{\bar{\nu}_e \rightarrow \bar{\nu}_e} = 1 - 16 \frac{(A + \bar{B})^4}{\bar{N}_1 \bar{N}_2^2} \sin^2 \left(\frac{1}{2} \Delta_{21} L \right). \quad (10)$$

At low energies, the A term in $h_{\text{eff}}^{\bar{\nu}}$ dominates. Using the low-energy limits $\bar{N}_1^2 \rightarrow 6A^2$, $\bar{N}_2^2 \rightarrow 3A^2$, we find for

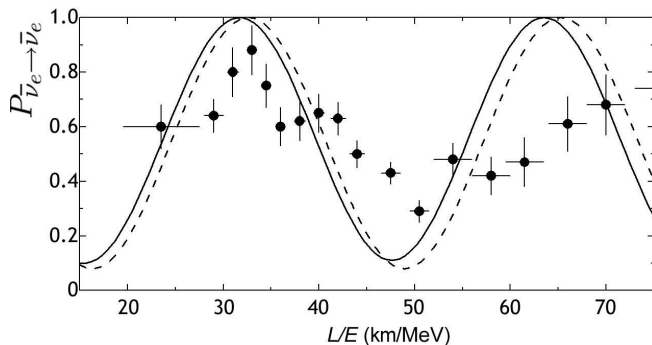


FIG. 4: Reactor-antineutrino survival probabilities as a function of L/E in the puma model (solid line) and in the $3\nu\text{SM}$ (dashed line). The data are from the long-baseline KamLAND experiment, for which $L \simeq 180$ km [54].

$P_{\bar{\nu}_e \rightarrow \bar{\nu}_e}$ the simple low-energy approximation

$$P_{\bar{\nu}_e \rightarrow \bar{\nu}_e} \approx 1 - \frac{8}{9} \sin^2 \left(\frac{3m^2 L}{4E} \right) \quad (\text{low energy}). \quad (11)$$

The fixed value $8/9$ for the oscillation amplitude matches expectations because at low energies $h_{\text{eff}}^{\bar{\nu}}$ is diagonalized using the tribimaximal mixing matrix. This result applies to reactor antineutrinos in both long- and short-baseline experiments. The large disappearance amplitude for reactor antineutrinos is evident in the $\bar{\nu}_e \rightarrow \bar{\nu}_e$ panel of Fig. 3.

1. Long-baseline reactor: KamLAND

In the $3\nu\text{SM}$, the reactor-antineutrino survival probability for long-baseline experiments is

$$P_{\bar{\nu}_e \rightarrow \bar{\nu}_e}^{3\nu\text{SM}} \approx 1 - \sin^2 2\theta_{12} \sin^2 \left(\frac{\Delta m_{\odot}^2 L}{4E} \right). \quad (12)$$

The data indicate values for the $3\nu\text{SM}$ parameters of $\sin^2 2\theta_{12} \simeq 0.92$ and $\Delta m_{\odot}^2 \simeq 7.58 \times 10^{-5} \text{ eV}^2$ [53]. Comparing the oscillation phase in this result with that in Eq. (11), we find that agreement with the KamLAND results can be achieved by choosing the mass parameter m^2 to be $m^2 = \Delta m_{\odot}^2/3$ [9]. This gives the numerical value adopted in Eq. (8). The match between the two models is shown in Fig. 4.

Notice that the disappearance of reactor antineutrinos is described using only one parameter m instead of the usual two in the $3\nu\text{SM}$. The conventional solar mixing angle θ_{12} is eliminated as a degree of freedom by the form of the texture h_{eff}^{ν} . Inspecting Eq. (11) reveals that at low energies the effective value of $\sin^2 2\theta_{12}$ is numerically fixed to $(\sin^2 2\theta_{12})_{\text{eff}} \simeq 0.89$, which is close to the measured magnitude. The reader is however cautioned that this interpretation fails at higher energies due to the energy dependence of the mixing in the puma model.

2. Short-baseline reactors

In recent years, numerous reactor experiments with short baselines $L \lesssim 1$ km such as Bugey ($L \simeq 15, 40$ m) [62], CHOOZ ($L \simeq 1$ km) [63], Gösgen ($L \simeq 38, 46, 65$ m) [64], and Palo Verde ($L \simeq 750, 890$ m) [65] have sought evidence for the disappearance of electron antineutrinos with null results. The explanations of these results differ qualitatively in the puma model and the $3\nu\text{SM}$.

In the $3\nu\text{SM}$, the $\bar{\nu}_e$ survival probability is

$$P_{\bar{\nu}_e \rightarrow \bar{\nu}_e}^{3\nu\text{SM}} \approx 1 - \sin^2 2\theta_{13} \sin^2 \left(\frac{\Delta m_{\text{atm}}^2 L}{4E} \right). \quad (13)$$

For energies $E \simeq 3$ MeV, this gives an antineutrino disappearance length $2\pi E/\Delta m_{\text{atm}}^2 \simeq 8.1 \times 10^{18} \text{ GeV}^{-1}$, which is about 1.5 km. The null experimental results are therefore interpreted in the $3\nu\text{SM}$ as a consequence of a small mixing angle θ_{13} . Note that the $3\nu\text{SM}$ survival probabilities (12) and (13) for long and short baselines, respectively, have the same form but involve four different parameters, $\Delta m_{\text{solar}}^2$, θ_{12} , Δm_{atm}^2 , and θ_{13} .

In contrast, in the puma model the oscillation probability (11) holds at low energies for any baseline. Only the single parameter m is required to describe both the long- and short-baseline data. For energies $E \simeq 3$ MeV, the antineutrino disappearance length is $\bar{L}_{21} \equiv \pi/\bar{\Delta}_{21} \simeq 2\pi E/\Delta m_{\odot}^2 \simeq 2.5 \times 10^{20} \text{ GeV}^{-1}$, which is about 50 km. The null reactor results are therefore understood in this model as a consequence of the short baselines, which limit the contribution of the oscillation phase to the survival probability, rather than a consequence of a small oscillation amplitude as in the $3\nu\text{SM}$. Indeed, the amplitude of the oscillating term in Eq. (11) is $8/9$, which is large.

Since the puma model contains no term with a phase involving Δm_{atm}^2 , we see that at low energies the effective value $(\sin^2 2\theta_{13})_{\text{eff}}$ of the $3\nu\text{SM}$ quantity $\sin^2 2\theta_{13}$ is exactly zero. This is a consequence of the zero value of U_{3e} , as can be confirmed by comparing the $3\nu\text{SM}$ mixing matrix with the tribimaximal limit of the mixing matrix (3). Note, however, that the energy dependence of the mixing matrix makes this result invalid at higher energies, where the effective value $(\sin^2 2\theta_{13})_{\text{eff}}$ extracted from high-energy experiments can be nonzero even though U_{3e} identically vanishes.

C. Solar neutrinos

For neutrinos propagating in matter, the effective hamiltonian h_{eff}^{ν} acquires an additional term [66]. The modified effective hamiltonian $(h_{\text{eff}}^{\nu})^{\text{M}}$ in the solar interior can be written as

$$(h_{\text{eff}}^{\nu})_{ab}^{\text{M}} = (h_{\text{eff}}^{\nu})_{ab} + V_{\odot} \delta_{ae} \delta_{be}, \quad (14)$$

where the solar matter potential V_{\odot} takes the value $V_{\odot} = \sqrt{2}G_{\text{F}}n_e \simeq 7.84 \times 10^{-21} \text{ GeV}$ at the solar core [67].

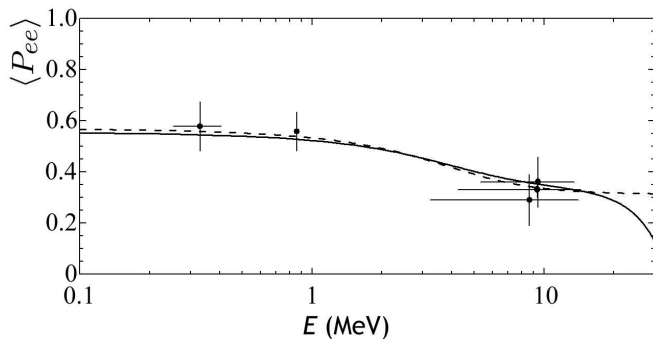


FIG. 5: Averaged survival probability for solar neutrinos in the puma model (solid line) and in the 3ν SM (dashed line). Both cases include matter-induced effects in the adiabatic approximation. The data are from Ref. [52].

The presence of the solar potential preserves the puma texture (1) because it corresponds to a simple redefinition of the function C of the form $C \rightarrow C + V_\odot$. The exact eigenvalues and the exact mixing matrix in the presence of matter can therefore be found immediately by applying this redefinition to Eqs. (2), (3), and (4). A short calculation reveals that the averaged survival probability of solar neutrinos takes the exact form

$$\langle P_{\nu_e \rightarrow \nu_e} \rangle = \left(\frac{(\lambda_1^M - 2A)(\lambda_1 - 2A)}{N_1^M N_1} \right)^2 + \left(\frac{(\lambda_2^M - 2A)(\lambda_2 - 2A)}{N_2^M N_2} \right)^2. \quad (15)$$

For the lower-energy region of the solar spectrum with $E \sim 0.1$ MeV, the solar potential V_\odot and the functions B and C are negligible. In this limit, the averaged survival probability becomes

$$\langle P_{\nu_e \rightarrow \nu_e} \rangle \approx \sum_{a'} |U_{a'e}|^4 = \frac{5}{9} \quad (\text{low energy}), \quad (16)$$

in agreement with the data. This result is to be expected because the vacuum mixing matrix is tribimaximal at low energies.

For higher energies, the solar potential and the Lorentz-violating terms can introduce novel effects, depending on the form of the functions B and C . The detailed form of the averaged survival probability therefore becomes model dependent. However, the neutrino survival probability initially drops below the limiting value $5/9$ as the energy increases. This generic effect is a consequence of the energy independence of V_\odot , which ensures V_\odot becomes relevant at energies comparable or below those for the Lorentz-violating terms and thereby enhances the disappearance of ν_e .

The above features are visible in Fig. 5. The solid line displays the averaged survival probability for the values (8). The curve is similar to that obtained from the 3ν SM and is compatible with observations.

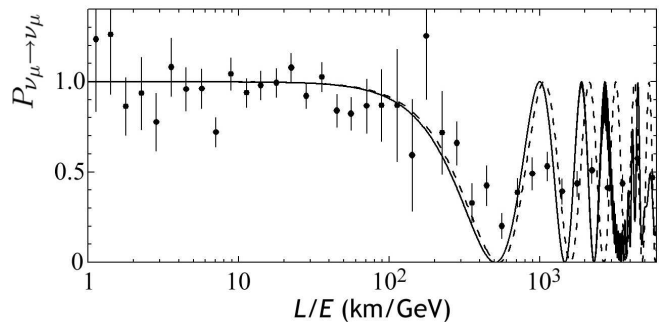


FIG. 6: Survival probability for atmospheric neutrinos as a function of L/E in the puma model (solid line) and in the 3ν SM (dashed line) compared to SK data, for which $L_{\text{SK}} \simeq 600$ km [60].

D. Atmospheric neutrinos

In the puma model, the exact survival probability of atmospheric neutrinos is

$$P_{\nu_\mu \rightarrow \nu_\mu} = 1 - 4 \frac{(A+B)^4}{N_1^2 N_2^2} \sin^2 \left(\frac{1}{2} \Delta_{21} L \right) - 2 \frac{(A+B)^2}{N_1^2} \sin^2 \left(\frac{1}{2} \Delta_{31} L \right) - 2 \frac{(A+B)^2}{N_2^2} \sin^2 \left(\frac{1}{2} \Delta_{32} L \right). \quad (17)$$

However, as E grows the A term becomes negligible, so the sole mass parameter m is irrelevant for high-energy oscillations. Requiring C to increase with energy faster than B yields the high-energy limits $\lambda_1 \rightarrow -2B^2/C$, $\lambda_2 \rightarrow C$, $N_1^2 \rightarrow 2B^2$, and $N_2^2 \rightarrow C^2$. The electron-neutrino content then lies exclusively in the second eigenstate. This leaves the other two uniformly populated by ν_μ and ν_τ , as can be verified by examining Fig. 2. The survival probability (17) then takes the simple form

$$P_{\nu_\mu \rightarrow \nu_\mu} \approx 1 - \sin^2 \left(\frac{B^2 L}{C} \right) \quad (\text{high energy}) \\ \approx 1 - \sin^2 \left(\frac{(\overset{\circ}{k}^{(p)})^2 L}{\overset{\circ}{c}^{(q)} E} \right), \quad (18)$$

where in the second equation the leading contributions to B and C are expressed as monomials of the form (5). Note that the unit amplitude of the oscillation term implies maximal mixing, as discussed following Eq. (6).

In contrast, the 3ν SM survival probability for atmospheric neutrinos takes the form

$$P_{\nu_\mu \rightarrow \nu_\mu}^{3\nu\text{SM}} \simeq 1 - \sin^2 2\theta_{23} \sin^2 \left(\frac{\Delta m_{\text{atm}}^2 L}{4E} \right) \quad (19)$$

depending on two parameters θ_{23} and Δm_{atm}^2 . Experimental data provide the values $\sin^2 2\theta_{23} > 0.90$ and

$|\Delta m_{\text{atm}}^2| \simeq 2.32 \times 10^{-3} \text{ eV}^2$ [57]. Comparison of Eqs. (18) and (19) suggests agreement with atmospheric data can be obtained when the ratio of $(\hat{k}^{(p)})^2$ and $\hat{c}^{(q)}$ satisfies

$$\frac{(\hat{k}^{(p)})^2}{\hat{c}^{(q)}} = \frac{1}{4} \Delta m_{\text{atm}}^2. \quad (20)$$

This condition has been used to constrain the coefficients $\hat{a}^{(5)}$ and $\hat{c}^{(8)}$ in Eq. (8) [9]. The resulting match between the two models is shown in Fig. 6 along with SK data.

Note that the ratio (20) represents only one degree of freedom. Nonetheless, it suffices to reproduce the data for atmospheric neutrinos via Eq. (18). The other degree of freedom in the two coefficients $\hat{k}^{(p)}$, $\hat{c}^{(q)}$ determines the onset of the Lorentz-violating seesaw. Increasing $\hat{c}^{(q)}$ while holding fixed the ratio (20) causes the seesaw to trigger at lower energies.

E. Short-baseline accelerator neutrinos

At high energies $E \gtrsim 1 \text{ GeV}$, a variety of short-baseline experiments have reported null results. BNL-E776 ($L = 1 \text{ km}$) searched for $\nu_\mu \rightarrow \nu_e$ and $\bar{\nu}_\mu \rightarrow \bar{\nu}_e$ at 1 GeV [68]. CCFR ($L \simeq 1 \text{ km}$) searched for $\nu_\mu \rightarrow \nu_e$, $\bar{\nu}_\mu \rightarrow \bar{\nu}_e$, $\nu_e \rightarrow \nu_\tau$, and $\bar{\nu}_e \rightarrow \bar{\nu}_\tau$ at 140 GeV [69]. CDHS ($L \simeq 130 \text{ m}$) searched for ν_μ disappearance at 1 GeV [70]. CHORUS ($L \simeq 600 \text{ m}$) searched for $\nu_\mu \rightarrow \nu_\tau$ at 27 GeV [71]. NOMAD ($L \simeq 600 \text{ m}$) searched for $\nu_\mu \rightarrow \nu_\tau$ and $\nu_e \rightarrow \nu_\tau$ at 45 GeV [72]. NuTeV ($L \simeq 1 \text{ km}$) searched for $\nu_\mu \rightarrow \nu_e$ and $\bar{\nu}_\mu \rightarrow \bar{\nu}_e$ at 150 GeV [73].

The puma model is consistent with all these null results. For energies above the seesaw scale $\sim 1 \text{ GeV}$, $\nu_\mu \leftrightarrow \nu_\tau$ mixing becomes maximal by construction, as described following Eq. (6). This feature implies vanishing high-energy mixing and hence no oscillations in the channels $\nu_\mu \rightarrow \nu_e$, $\bar{\nu}_\mu \rightarrow \bar{\nu}_e$, $\nu_e \rightarrow \nu_\tau$, and $\bar{\nu}_e \rightarrow \bar{\nu}_\tau$. The behavior can be seen directly from Fig. 3, which displays the energy dependence of the oscillation amplitudes.

In the $\nu_\mu \rightarrow \nu_\tau$ channel, the oscillation amplitude is maximal at high energies. However, the oscillation phase is controlled by Δ_{21} , which generates an appearance length L_{21} of several hundred kilometers at 1 GeV. The lack of a signal in this channel in the CHORUS or NOMAD data is therefore understood here as a consequence of their short baselines.

F. MiniBooNE anomalies

Two results from the MiniBooNE experiment indicate possible oscillation effects that cannot be accommodated within the $3\nu\text{SM}$. For neutrino oscillations $\nu_\mu \rightarrow \nu_e$, MiniBooNE finds a 3σ excess of events at low energies around 200-500 MeV [5]. For antineutrino oscillations $\bar{\nu}_\mu \rightarrow \bar{\nu}_e$, a 1.3σ low-energy excess has also been reported [6], with recent preliminary data suggesting a larger excess [74].

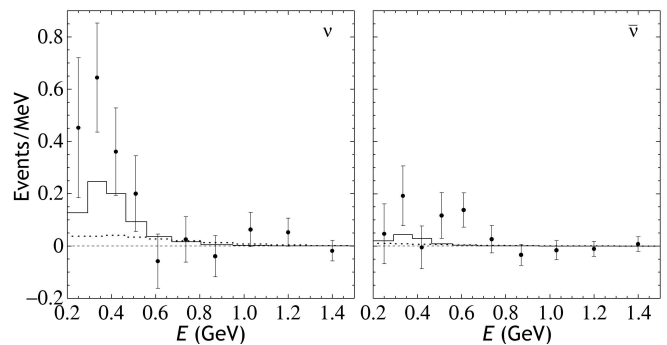


FIG. 7: Comparison of the puma model (solid lines; $\chi_\nu^2 = 1.0$, $\chi_{\bar{\nu}}^2 = 0.9$), the tandem model [19] (dotted lines; $\chi_\nu^2 = 1.9$, $\chi_{\bar{\nu}}^2 = 1.0$), and the $3\nu\text{SM}$ (dashed lines; $\chi_\nu^2 = 2.2$, $\chi_{\bar{\nu}}^2 = 1.1$), with MiniBooNE neutrino [5] and antineutrino [6] data.

These results are interesting in the present context because they lie in the energy region where the seesaw mechanism is triggered. Following onset of the seesaw, the eigenvalue λ_1 decreases linearly with energy while λ_2 grows rapidly. The appearance length $L_{21} \propto (\lambda_2 - \lambda_1)^{-1}$ therefore drops steeply, becoming a few hundred meters at MiniBooNE energies. This produces a large oscillation phase and hence a signal in the experiment. However, the oscillation amplitude for $\nu_\mu \leftrightarrow \nu_e$ mixing rapidly goes to zero as the $\nu_\mu \leftrightarrow \nu_\tau$ mixing becomes maximal, as can be seen in Fig. 3. As a result, the appearance signal in MiniBooNE vanishes at higher energies.

The puma model therefore naturally describes a low-energy excess in MiniBooNE. Moreover, the excess can differ substantially for neutrinos and antineutrinos when a coefficient for CPT-odd Lorentz violation is involved, such as occurs for the $c_8 a_5 m$ example (8). In general, the energy at which the excess appears depends on the seesaw scale and becomes smaller as $\hat{c}^{(q)}$ increases. For the values (8), the match to data is shown in Fig. 7.

We emphasize that these interesting features of the model arise without introducing additional particles or forces. They are a consequence of the comparatively elegant texture (1) that describes all compelling neutrino-oscillation data.

IV. PREDICTIONS

The discussion in the previous sections demonstrates that two of the three parameters of the model (1) suffice to reproduce all the compelling data for neutrino and antineutrino oscillations, while the third accommodates the two MiniBooNE anomalies. Comparison to the $3\nu\text{SM}$, which uses five nonzero parameters to describe established results but cannot reproduce the MiniBooNE anomalies, suggests the puma model offers a frugal interpretation of known data.

The model predicts a variety of signals, some of which

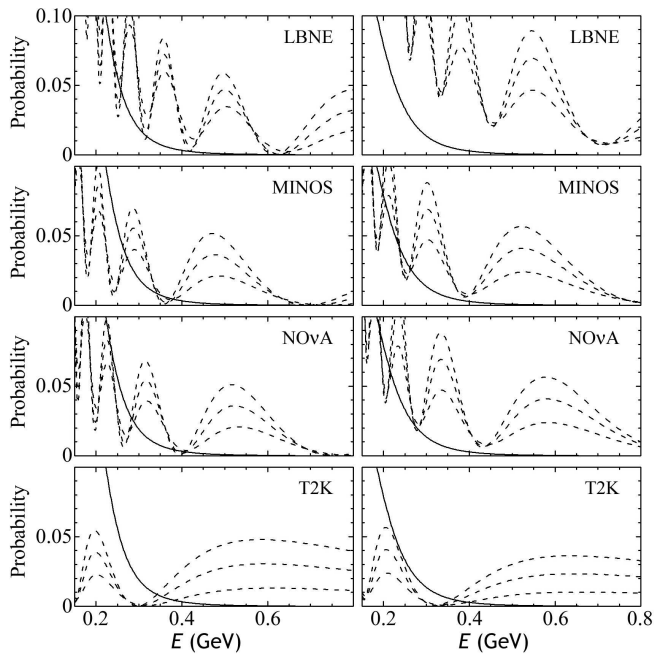


FIG. 8: Prediction for the probabilities of ν_e appearance (left) and of $\bar{\nu}_e$ appearance (right) in various long-baseline experiments according to the puma model (solid lines) and the 3ν SM (upper dashed lines, $\sin^2 2\theta_{13} = 0.02$; middle dashed lines, $\sin^2 2\theta_{13} = 0.05$; lower dashed lines, $\sin^2 2\theta_{13} = 0.08$). Matter effects are included.

differ qualitatively from 3ν SM expectations. In this section, we address some features of relevance to future experiments.

A. Long-baseline neutrinos

A variety of long-baseline experiments, including LBNE ($L \simeq 1300$ km) [75], MINOS ($L \simeq 735$ km) [76], NO ν A ($L \simeq 810$ km) [77], and T2K ($L \simeq 298$ km) [78], have design capabilities to search for ν_e appearance in a ν_μ beam. These searches are motivated in part by the prospects of measuring the 3ν SM parameter θ_{13} . No such parameter exists in the model (1), but signals in these experiments may nonetheless appear.

To characterize potential signals in the puma model, recall that the appearance length L_{21} for $\nu_\mu \rightarrow \nu_e$ decreases steeply with energy due to the seesaw mechanism. Baselines $L \gg L_{21}$ therefore involve rapid oscillations, so accelerator experiments with long baselines can observe only the averaged oscillation probability, given exactly by

$$\langle P_{\nu_\mu \rightarrow \nu_e} \rangle = 4 \frac{(A+B)^4}{(N_1^M N_2^M)^2}. \quad (21)$$

To allow for matter effects on neutrinos traversing the Earth, N_1^M and N_2^M are given by Eq. (4) with the re-

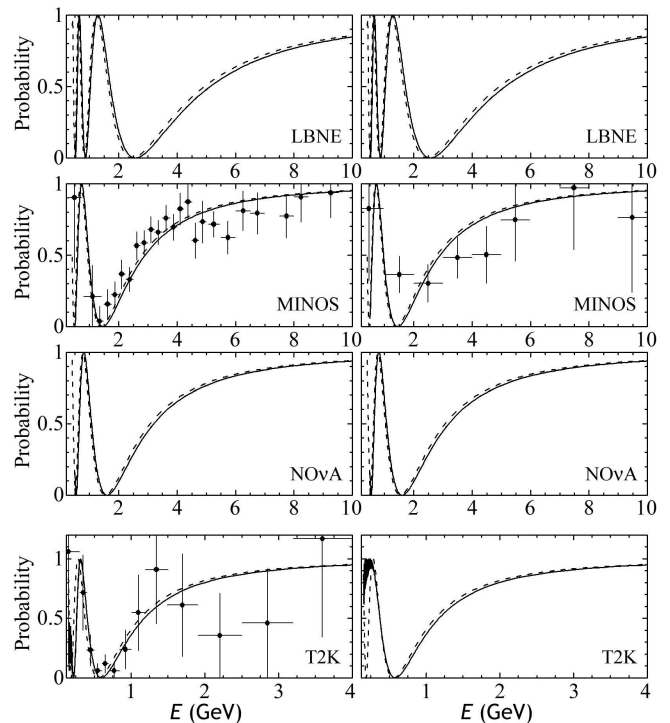


FIG. 9: Prediction for the probabilities of ν_μ disappearance (left) and of $\bar{\nu}_\mu$ disappearance (right) in various long-baseline experiments according to the puma model (solid lines) and the 3ν SM (dashed lines). Matter effects are included. The data are taken from Refs. [7, 57, 79].

placement $C \rightarrow C + V_\oplus$, where the Earth's matter potential V_\oplus is $V_\oplus \simeq 1.2 \times 10^{-22}$ GeV.

For energies above the seesaw scale, $\nu_\mu \leftrightarrow \nu_\tau$ mixing dominates while $\nu_\mu \leftrightarrow \nu_e$ mixing is highly suppressed. However, to describe the SK and MINOS data, the seesaw must trigger below 1 GeV. This means only small signals from $\nu_\mu \rightarrow \nu_e$ transitions can appear in the high-energy experiments LBNE, MINOS, and NO ν A. In contrast, T2K runs at lower energies, and so a larger appearance signal that decreases rapidly with the energy is to be expected. Quantitative predictions for the probabilities for ν_e and $\bar{\nu}_e$ appearance in the various experiments are shown in Fig. 8 for the values (8). Note that matter effects are almost negligible compared to the large eigenvalue λ_2 controlling the mixing, whereas for the 3ν SM curves they induce substantial differences between the probabilities for ν_e and $\bar{\nu}_e$ appearance.

We remark in passing that attempting to interpret these signals as arising from a nonzero 3ν SM angle θ_{13} would predict that θ_{13} is larger in T2K than in the other higher-energy experiments. This is compatible with recent results for ν_e appearance [2]. Note also that within this perspective the effective values of θ_{13} obtained with long-baseline accelerators are unrelated to the effective values of θ_{13} extracted from studies of reactor antineu-

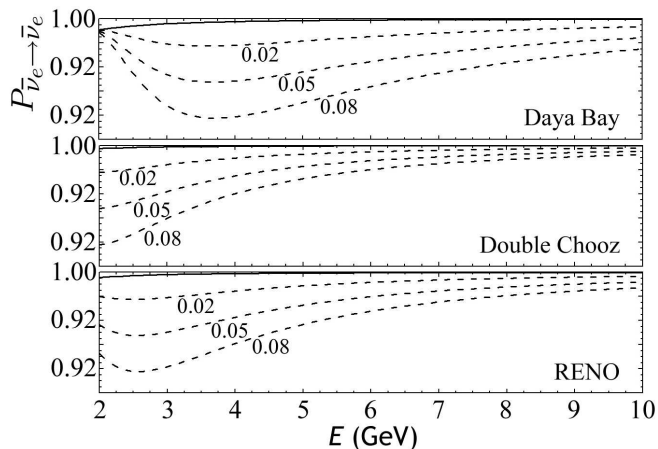


FIG. 10: Predictions for the probability of $\bar{\nu}_e$ disappearance in the Daya Bay, Double Chooz, and RENO experiments according to the puma model (solid lines) and the 3ν SM (dashed lines, labeled with the value of $\sin^2 2\theta_{13}$).

trinos discussed in Sec. III B 2.

High-energy long-baseline experiments can also perform precision studies of ν_μ disappearance. For this oscillation channel, no differences between the puma model and the 3ν SM are expected in LBNE, MINOS, and NO ν A because they operate at energies above the seesaw scale. However, significant differences between neutrinos and antineutrinos are predicted for the lower-energy portion of the T2K spectrum when the theory contains a coefficient for CPT-odd Lorentz violation, as in the $c_8 a_5 m$ model. The predictions are displayed in Fig. 9, where as before the values (8) are used for illustration.

B. Short-baseline neutrinos

Using baselines in the range 1-2 km, modern reactor experiments such as Daya Bay ($L \simeq 1985$ m) [80], Double Chooz ($L \simeq 1050$ m) [81], and RENO ($L \simeq 1380$ m) [82] propose to measure the disappearance of reactor antineutrinos. Like their long-baseline cousins, these experiments are driven partly by prospects for measuring the 3ν SM mixing angle θ_{13} .

In the puma model, the $\bar{\nu}_e$ survival probability for energies 2-9 MeV has a large amplitude, as can be seen from Eq. (11). The oscillation signal in a given reactor experiment therefore depends only on the size of the baseline L compared to the antineutrino disappearance length $\bar{L}_{21} \simeq 50$ km discussed in Sec. III B 2. The baselines for the Daya Bay, Double Chooz, and RENO experiments are all short compared to this, with Daya Bay having the greater sensitivity to oscillation signals due to its longer baseline. Since \bar{L}_{21} grows linearly with the energy, any oscillation signal in these experiments is expected to appear predominantly at low energies. Using

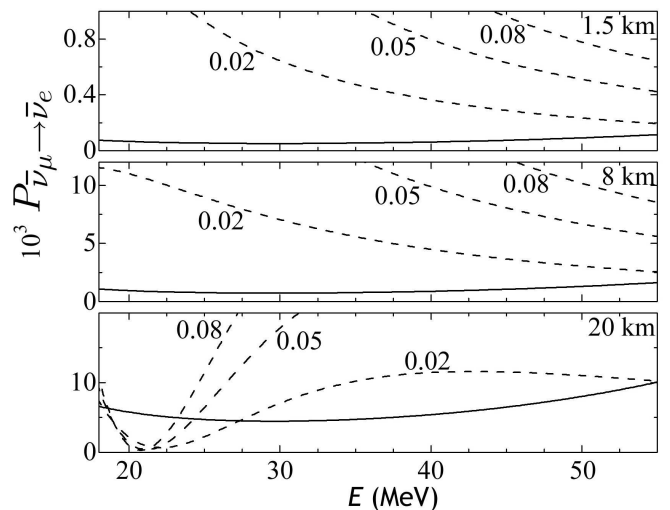


FIG. 11: Predictions for the probability of $\bar{\nu}_e$ appearance at the three baselines proposed for the DAE δ ALUS experiment according to the puma model (solid lines) and the 3ν SM (dashed lines, labeled with the value of $\sin^2 2\theta_{13}$).

the model values (8), the predictions for the disappearance probabilities in the three experiments are shown in Fig. 10.

We note in passing that the recent suggestion of an overestimation of antineutrino fluxes in short-baseline reactor experiments [83] is difficult to reconcile with the three-parameter puma model. Since effects at low energies are governed by only one parameter m , which is fixed by KamLAND data, no other oscillation length appears at reactor energies. The existence of only one parameter is a consequence of the S_3 flavor symmetry, so a slight breaking of this symmetry at low energies could accommodate an additional parameter and hence a corresponding signal. This construction would introduce another degree of freedom but requires no additional neutrinos. However, investigations along these lines lie beyond the scope of the present work.

Another experiment of interest in the context of short-baseline neutrinos is the recent DAE δ ALUS proposal [84] to study CP violation, which would generate neutrinos at several different baseline distances from a detector using high-power accelerator modules to beam protons onto graphite sources. A popular configuration would offer the capability to search for $\bar{\nu}_\mu \rightarrow \bar{\nu}_e$ transitions using three baselines of about 1.5 km, 8 km, and 20 km. The large oscillation amplitude in this region suggests appearance signals in the detector can be expected from the more distant sources. The predicted appearance probabilities for the three proposed baselines are shown in Fig. 11.

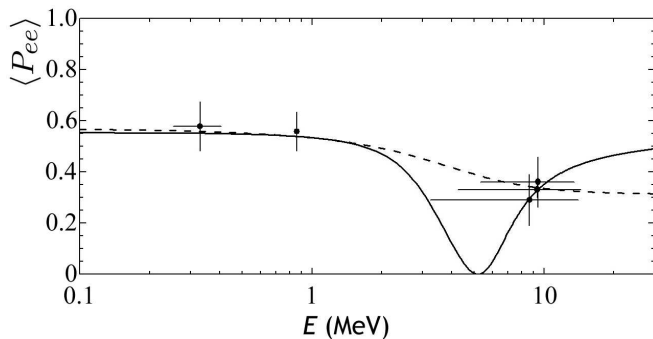


FIG. 12: Averaged survival probability for solar neutrinos in the c_4a_3m model (solid line) and in the 3ν SM (dashed line). Both cases include matter-induced effects in the adiabatic approximation. The data are taken from Ref. [52].

V. VARIANT PUMA MODELS

In the preceding sections, the implications of the general texture (1) have been illustrated with the c_8a_5m model, using the specific values (8). However, other models can be constructed using h_{eff}^ν that successfully describe most or all compelling neutrino data. Some of these offer distinctive features or intriguing possibilities for describing experimental anomalies beyond the MiniBooNE ones. This section outlines some results for a few of these variant models.

A. The c_4a_3m model

The texture h_{eff}^ν with the smallest monomial orders p and q in Eq. (5) requires only renormalizable operators of dimensions 3 and 4 in the minimal SME, hence producing a c_4a_3m model. For definiteness, we adopt in this subsection the specific numerical values

$$\begin{aligned} m^2 &= 2.6 \times 10^{-23} \text{ GeV}^2, \\ \hat{a}^{(3)} &= -2.5 \times 10^{-21} \text{ GeV}, \\ \hat{c}^{(4)} &= 1.0 \times 10^{-20}. \end{aligned} \quad (22)$$

As mentioned at the end of Sec. II, we use a zero ee entry in the B term for this model. The coefficient $\hat{a}^{(3)}$ comes with CPT violation, so differences between neutrino and antineutrino properties can be expected. These values are consistent with limits from direct mass measurements, cosmological mass bounds, and constraints on anisotropic oscillations.

The c_4a_3m model is compatible with all accepted experimental oscillation results discussed in Sec. III, including those obtained with reactor, solar, and atmospheric neutrinos. However, the eigenvalue λ_2 grows too slowly to produce a signal in MiniBooNE because the function C is linear in energy.

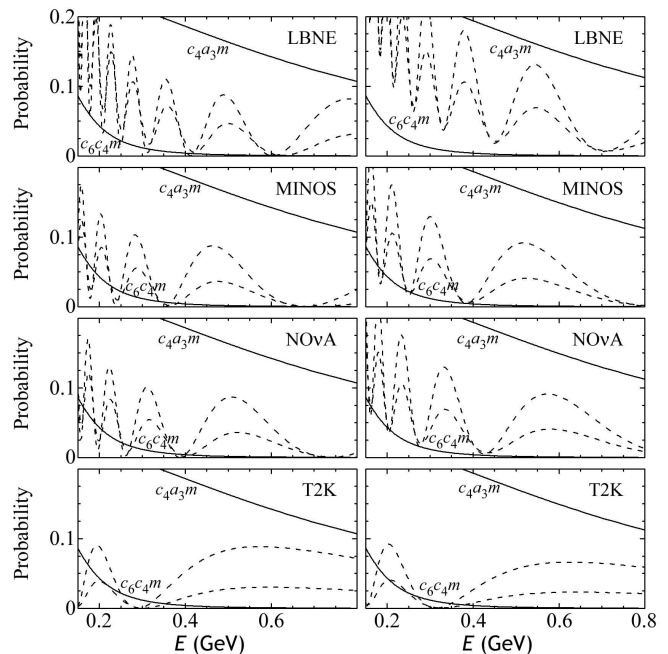


FIG. 13: Prediction for the probabilities of ν_e appearance (left) and of $\bar{\nu}_e$ appearance (right) in various long-baseline experiments according to variant puma models (solid lines, labeled by the model) and the 3ν SM (upper dashed lines, $\sin^2 2\theta_{13} = 0.15$; lower dashed lines, $\sin^2 2\theta_{13} = 0.05$). Matter effects are included.

An interesting qualitative difference introduced by the model appears in the predicted averaged survival probability for solar neutrinos, shown in Fig. 12. The probability curve incorporates a striking neutrino-disappearance maximum in the central-energy region, despite passing through all data points. This reflects the importance at lower energies of the coefficient $\hat{a}^{(3)}$, an effect absent for the $\hat{a}^{(5)}$ coefficient in the c_8a_5m model. The curve shape suggests future analyses of solar data in the 1-10 MeV part of the neutrino spectrum could provide an interesting experimental test of the model.

Another distinctive feature of the model is a large signal for $\nu_\mu \rightarrow \nu_e$ oscillations in long-baseline experiments. The signal decreases with energy, as shown in Fig. 13. Analysis of the recent data supporting electron-neutrino appearance in the T2K and MINOS experiments [2] could provide a sharp constraint on this signal, potentially excluding the values (22).

B. The c_6c_4m model

Other interesting variant models can be constructed using only CPT-even operators. Using monomials of smallest order produces a c_6c_4m model. We choose here

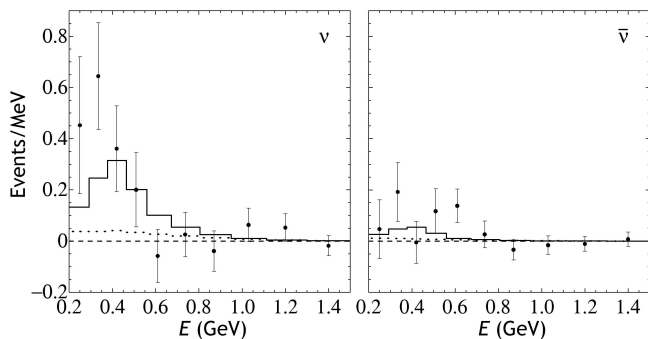


FIG. 14: Comparison of the c_6c_4m model (solid lines; $\chi_\nu^2 = 1.0$, $\chi_{\bar{\nu}}^2 = 0.8$), the tandem model [19] (dotted lines; $\chi_\nu^2 = 1.9$, $\chi_{\bar{\nu}}^2 = 1.0$), and the 3ν SM (dashed lines; $\chi_\nu^2 = 2.2$, $\chi_{\bar{\nu}}^2 = 1.1$), with MiniBooNE neutrino [5] and antineutrino [6] data.

the specific numerical values

$$\begin{aligned} m^2 &= 2.6 \times 10^{-23} \text{ GeV}^2, \\ \tilde{c}^{(4)} &= 7.7 \times 10^{-20}, \\ \tilde{c}^{(6)} &= 1.0 \times 10^{-17} \text{ GeV}^{-2}. \end{aligned} \quad (23)$$

As for other examples considered in this work, these values are consistent with limits from direct mass measurements, cosmological mass bounds, and constraints on anisotropic oscillations.

Like the c_8a_5m and c_4a_3m models, the c_6c_4m model provides a good match to the data from reactor, solar, and atmospheric neutrinos discussed in Sec. III. The presence of the $\tilde{c}^{(4)}$ term substantially affects the physics in the region 10 MeV to 1 GeV. It generates a signal in the MiniBooNE region that includes low-energy excesses in both neutrinos and antineutrinos, as shown in Fig. 14. Note the asymmetry in the signal, which here reflects experimental acceptance rather than CPT violation.

For ν_e appearance in long-baseline experiments, the probabilities are generically closer in magnitude to those of the 3ν SM with a moderate value of θ_{13} , as shown in Fig. 13. One interesting feature is the substantially larger signal produced in T2K relative to MINOS, which is compatible with the central values of recently reported measurements [2].

C. Four-coefficient models

Some indication of a potential difference between ν_μ and $\bar{\nu}_\mu$ disappearance probabilities has recently been reported by the MINOS collaboration [7]. Although the effect may disappear with improved statistics, a difference of this kind is of interest in the present context because it cannot be accommodated in the 3ν SM, which requires identical neutrino and antineutrino masses.

In three-parameter puma models, the survival probabilities of muon neutrinos and antineutrinos at MINOS

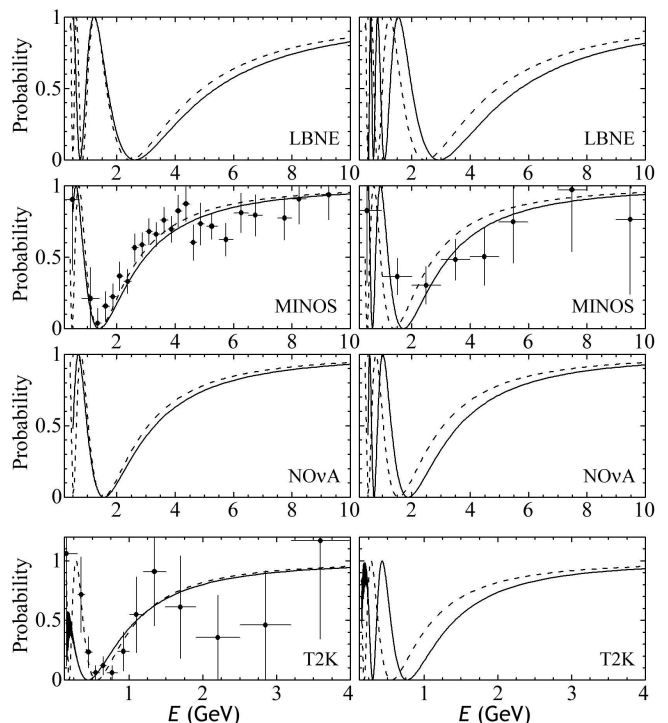


FIG. 15: Prediction for the probabilities of ν_μ disappearance (left) and of $\bar{\nu}_\mu$ disappearance (right) in various long-baseline experiments according to the $c_8a_5c_4m$ model (solid lines; $\chi_\nu^2 = 1.4$, $\chi_{\bar{\nu}}^2 = 0.9$ for MINOS) and the 3ν SM (dashed lines; $\chi_\nu^2 = 1.0$, $\chi_{\bar{\nu}}^2 = 1.6$ for MINOS). Matter effects are included. The data are taken from Refs. [7, 57, 79].

energies are generically the same. The result holds because at high energies the relevant eigenvalue difference is $\Delta_{31} \approx 2B^2/C$. This is even under CPT provided the B term is either odd or even, which is true whenever the B term is only a monomial in E . For the c_8a_5m model for example, this symmetry is reflected in Fig. 9. These puma models therefore cannot accommodate anomalies of the MINOS type either.

In this subsection, we show that an *ad hoc* modification using an additional parameter can describe anomalies of this type. The key idea is as follows. Instead of choosing a monomial in energy for the B term, we can take a binomial involving two different monomial orders p and $r < p$, one even and one odd. This produces a four-coefficient model with both CPT-odd and CPT-even terms contributing at high energies. If the value of r is close to p and the corresponding coefficients are similar in size, then the oscillation probabilities for neutrinos and antineutrinos differ at high energies. In particular, the energies of the first oscillation maxima of neutrinos and antineutrinos differ, which is a feature of the MINOS effect. However, to preserve compatibility with other experiments, the ee entry of the effective hamiltonian h_{eff}^ν must remain unchanged. The extra coefficient should

therefore appear only in the $e\mu$ and $e\tau$ entries of h_{eff}^ν . One way to achieve this is to choose a binomial for the C term as well, compensating for the modification of the ee entry arising from the change to B .

As an example, we can add a fourth coefficient to the $c_8 a_5 m$ model while leaving unchanged its main features. Choosing $r = 4$, which satisfies the requirement $r < p = 5$ with r near p , the fourth coefficient can be denoted $\tilde{c}^{(4)}$. To generate a neutrino-antineutrino difference at high energies, it suffices to redefine the B and C terms as $B \rightarrow B + \tilde{c}^{(4)} E$, $C \rightarrow C - \tilde{c}^{(4)} E$. For definiteness, we can take the numerical values

$$\begin{aligned} m^2 &= 2.6 \times 10^{-23} \text{ GeV}^2, \\ \tilde{c}^{(4)} &= 2.0 \times 10^{-20}, \\ \tilde{a}^{(5)} &= -2.6 \times 10^{-19} \text{ GeV}^{-1}, \\ \tilde{c}^{(8)} &= 1.0 \times 10^{-16} \text{ GeV}^{-4}, \end{aligned} \quad (24)$$

which as before are consistent with limits from direct mass measurements, cosmological mass bounds, and constraints on anisotropic oscillations. These choices preserve the attractive features of the simpler $c_8 a_5 m$ model.

The introduction of the fourth coefficient primarily affects the probabilities of ν_μ and $\bar{\nu}_\mu$ disappearance in long-baseline experiments, as shown in Fig. 15 for the values (24). In particular, the MINOS data in Ref. [7] are reasonably described by the model. The location of the primary minimum for antineutrino oscillations is at a higher energy than that for neutrinos, in agreement with the reported effect. We emphasize that this result is achieved with a single additional parameter, without any masses, in a global model of neutrino oscillations. Note also that this $c_8 a_5 c_4 m$ model predicts a large difference between the probabilities of ν_μ and $\bar{\nu}_\mu$ disappearance in the T2K experiment. However, the ν_e appearance probabilities in long-baseline experiments are essentially unchanged from those for the $c_8 a_5 m$ model shown in Fig. 8.

D. Enhanced models

In a search for appearance of electron antineutrinos in a beam of muon antineutrinos, the LSND experiment found evidence for a small probability $P_{\bar{\nu}_\mu \rightarrow \bar{\nu}_e} \simeq 0.26 \pm 0.08\%$ of $\bar{\nu}_\mu \rightarrow \bar{\nu}_e$ oscillations at baseline $L = 30$ m and energies in the range 20-60 MeV [4]. This signal cannot be accommodated within the $3\nu\text{SM}$ because the required mass-squared difference $\Delta m_{\text{LSND}}^2 \simeq 1 \text{ eV}^2$ is orders of magnitude larger than Δm_\odot^2 and Δm_{atm}^2 .

In the general puma model, the oscillation $\bar{\nu}_\mu \rightarrow \bar{\nu}_e$ is given exactly by

$$P_{\bar{\nu}_\mu \rightarrow \bar{\nu}_e} = 8 \frac{(A + \bar{B})^4}{N_1^2 N_2^2} \sin^2 \left(\frac{\bar{\Delta}_{21} L}{2} \right), \quad (25)$$

which is governed by the same eigenvalues that control reactor antineutrinos. The energies in the LSND experiment are greater than those of reactor antineutrinos, but

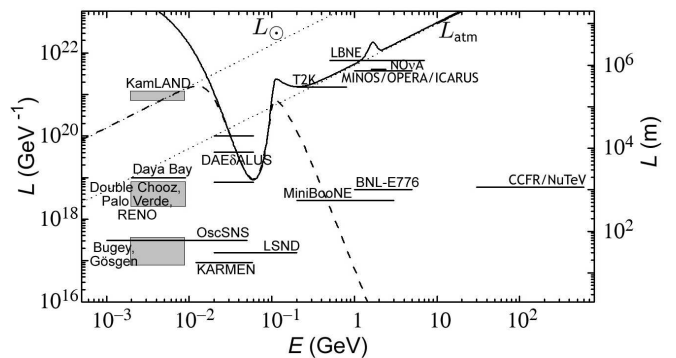


FIG. 16: Energy dependences of the oscillation lengths for antineutrinos in the doubly enhanced puma model. The corresponding plot for neutrinos in the top panel of Fig. 1 remains unaffected. The disappearance lengths for the model are \bar{L}_{31} (solid line) and \bar{L}_{21} (dashed line), displayed for the values given by Eqs. (24), (27), and (28). The dotted lines are the disappearance lengths L_\odot (solar) and L_{atm} (atmospheric) in the $3\nu\text{SM}$.

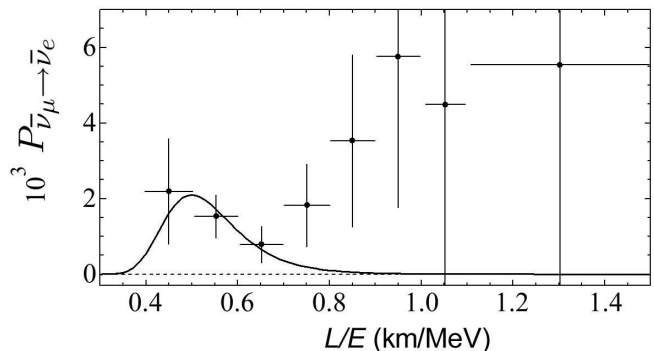


FIG. 17: Comparison of enhanced puma model (solid line, $\chi^2 = 1.6$) and the $3\nu\text{SM}$ (dashed line, $\chi^2 = 2.6$) with LSND antineutrino data [5].

the appearance length is smaller by about two orders of magnitude. Achieving this with a monomial energy dependence in h_{eff}^ν while preserving consistency with other experiments is challenging, as it requires a large power of the energy and a seesaw triggered around 10 MeV.

An interesting option generating the required steep fall and rise in $\bar{L}_{21}(E)$ is to introduce a smooth nonpolynomial function with a peak. A function of this type could act as an enhancement of h_{eff}^ν arising from a series of coefficients in the SME. It can be approximated generically using at least three parameters, one to position it, one to fix its height, and one to specify its width. A simple example is a gaussian enhancement of the form

$$\delta \bar{h} = \alpha \exp[-\beta(E - \varepsilon)^2]. \quad (26)$$

To preserve the S_2 symmetry of h_{eff}^ν , the enhancement can be limited to the $\bar{e}\bar{\mu}$ and $\bar{e}\bar{\tau}$ entries of h_{eff}^ν via the

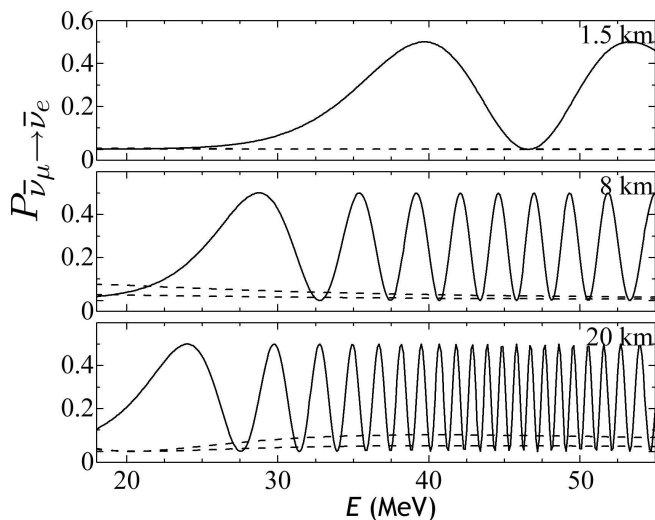


FIG. 18: Predictions for the probability of $\bar{\nu}_e$ appearance at the three baselines proposed for the DAE δ ALUS experiment according to the enhanced puma model (solid lines) and the 3ν SM (upper dashed lines, $\sin^2 2\theta_{13} = 0.15$; lower dashed lines, $\sin^2 2\theta_{13} = 0.05$).

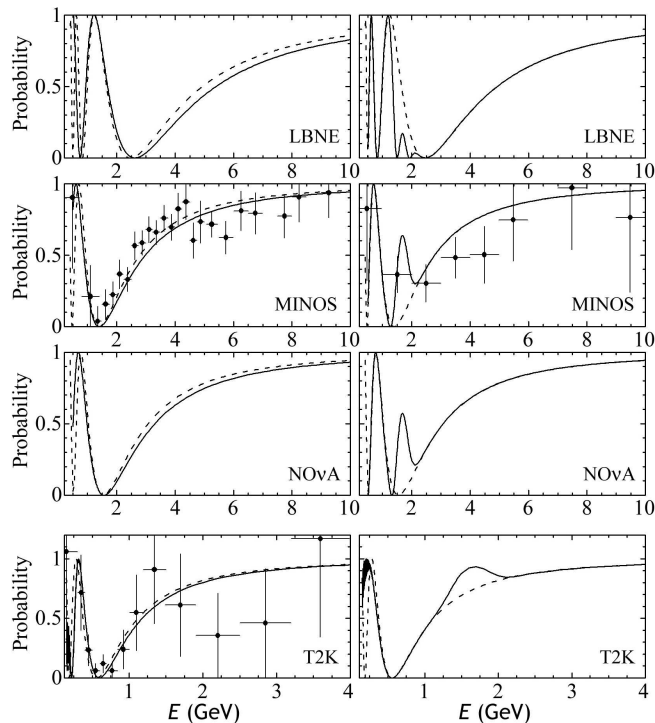


FIG. 19: Prediction for the probabilities of ν_μ disappearance (left) and of $\bar{\nu}_\mu$ disappearance (right) in various long-baseline experiments according to the doubly enhanced puma model (solid lines; $\chi_\nu^2 = 1.3$, $\chi_{\bar{\nu}}^2 = 0.9$ for MINOS) and the 3ν SM (dashed lines; $\chi_\nu^2 = 1.4$, $\chi_{\bar{\nu}}^2 = 1.8$ for MINOS). Matter effects are included. The data are taken from Refs. [7, 57, 79].

redefinitions $\bar{B} \rightarrow \bar{B} + \delta\bar{h}$ and $\bar{C} \rightarrow \bar{C} - \delta\bar{h}$. Under the CPT transformation mapping $h_{\text{eff}}^{\bar{\nu}}$ to h_{eff}^{ν} , the signs of α and ε change. As a result, either the function or its CPT conjugate is localized at an unphysical value of the energy, and so the enhancement affects either neutrinos or antineutrinos but not both.

As an example, consider an enhanced $c_8 a_5 m$ model with specific enhancement values

$$\begin{aligned}\alpha &= 3.0 \times 10^{-19} \text{ GeV}, \\ \beta &= 3.0 \times 10^3 \text{ GeV}^{-2}, \\ \varepsilon &= 60 \text{ MeV}.\end{aligned}\quad (27)$$

The positive value of ε ensures that only antineutrinos are affected. This enhancement produces a sharp dip in the disappearance length $\bar{L}_{21}(E)$ centered around 60 MeV, as displayed in Fig. 16. The resulting oscillation probability $P_{\bar{\nu}_\mu \rightarrow \bar{\nu}_e}$ contains a nonzero signal in the same region as the LSND data, as shown in Fig. 17. Since the \bar{L}_{21} curve passes through the region of sensitivity for the DAE δ ALUS experiment [84], large signals are predicted in all three detectors as shown in Fig. 18. A large oscillation signal is also predicted at high energies in the OscSNS experiment [85].

Differences between ν_μ and $\bar{\nu}_\mu$ disappearance probabilities can also be generated by another enhancement of this general type. Two simultaneous enhancements can be included without interference provided they are localized in different regions of the spectrum. Figure 16 shows the effect on the disappearance length \bar{L}_{31} of adding a second enhancement with the values

$$\begin{aligned}\alpha_2 &= -2.0 \times 10^{-19} \text{ GeV}, \\ \beta_2 &= 13 \text{ GeV}^{-2}, \\ \varepsilon_2 &= 1.7 \text{ GeV}.\end{aligned}\quad (28)$$

The resulting disappearance probabilities for muon neutrinos and antineutrinos in long-baseline experiments are shown in Fig. 19. While the single extra coefficient in the four-parameter $c_8 a_5 c_4 m$ model is more economical in generating an anomaly like that reported by MINOS [7], the introduction of the second enhancement centered near 2 GeV produces interesting and distinctive oscillation signals in the LBNE and NOvA experiments for ν_μ disappearance, as shown in Fig. 19. In contrast, the ν_e appearance probabilities displayed for the $c_8 a_5 m$ model in Fig. 8 are largely unaffected by the enhancement.

VI. DISCUSSION

In this work, we have investigated the behavior of neutrinos governed by an effective hamiltonian h_{eff}^ν of the puma form (1). This texture is interesting in part because it leads to descriptions of neutrino oscillations that are globally compatible with experimental data. The associated Lorentz-violating models are intriguing because they are frugal, they have a certain elegance, and their

novel features are compatible with data in unexpected ways. We remark in passing that the existence of these models was unclear *a priori*, becoming apparent only through a systematic search for viable candidates.

The frugality can be traced to the use of only two degrees of freedom to describe established data, instead of the usual five required by the 3ν SM, while a third degree of freedom efficiently encompasses the MiniBooNE anomalies. Adding a fourth degree of freedom readily generates an anomaly of the MINOS type, while a three-parameter enhancement produces a signal in the LSND experiment. These four latter degrees of freedom are *ad hoc*, and their necessity depends on the ultimate confirmation of the MINOS and LSND anomalies. However, to our knowledge the resulting texture represents the sole extant global model for neutrino oscillations, and moreover uses degrees of freedom comparable in number to those of the 3ν SM.

The symmetry of h_{eff}^ν also implies a certain elegance. The puma texture (1) could naturally stem from more fundamental physics at the unification scale that generates a democratic contribution to the dominant mass operator in the low-energy effective theory. The resulting S_3 symmetry then holds at low energies and ensures tribimaximal mixing but is broken to S_2 at higher energies by subdominant terms in the SME. This symmetry structure leads to the attractive quadratic calculability of the models. The coefficients required for compatibility with data are of plausible Planck-suppressed size.

The novel features of the puma models originate in the unconventional energy dependence in the eigenvalues of h_{eff}^ν and the mixing matrix U . Indeed, it is a pleasant surprise that the models pass the test of compatibility with existing data, despite their qualitative differences compared to the 3ν SM. One striking feature is the Lorentz-violating seesaw, which makes viable the absence of a mass parameter at high energies. Another satisfying feature is the steep drop with energy of the oscillation length L_{21} , which is naturally enforced by the third degree of freedom required to generate the Lorentz-violating see-

saw. As discussed above, this drop enables L_{21} to attain the vicinity of the MiniBooNE experiment in E - L space, thereby generating a low-energy signal compatible with the MiniBooNE anomaly. Moreover, this feature appears in conjunction with a rapid decrease in the relevant oscillation amplitudes accompanying the large oscillation phase. This accounts for null signals in high-energy short-baseline accelerator experiments without invoking the tiny oscillation phase of the 3ν SM.

The puma texture h_{eff}^ν predicts certain signals that differentiate sharply between it and the 3ν SM. One key feature is the energy dependence of the effective mixing angle θ_{13} . This implies the probability of ν_e appearance is larger in the T2K experiment than in the MINOS experiment. It also predicts no accompanying signal in reactor experiments, a result at odds with the 3ν SM. With an enhancement present, strong signals are predicted in experiments at intermediate energies and moderate baselines such as the proposed DAE δ ALUS experiment. Another unique signal predicted by some models is CPT violation, which implies differences in oscillation probabilities between neutrinos and antineutrinos. Perhaps the most direct evidence for Lorentz violation would be the discovery of oscillation anisotropies arising from the boost relative to the isotropic frame. One signal would be sidereal variations of oscillations in the laboratory frame [42], which in the puma models are predicted to be some 10-100 times below current sensitivities [9]. In any event, the results in this work show that Lorentz- and CPT-violating models can serve as an experimentally viable foil to the 3ν SM, while offering a simple and credible alternative for realistic modeling of neutrino oscillations.

Acknowledgments

This work was supported in part by the Department of Energy under grant DE-FG02-91ER40661 and by the Indiana University Center for Spacetime Symmetries.

-
- [1] K. Nakamura *et al.*, J. Phys. G **37**, 075021 (2010).
 - [2] T2K Collaboration, K. Abe *et al.*, Phys. Rev. Lett. **107**, 041801 (2011); MINOS Collaboration, P. Adamson *et al.*, arXiv:1108.0015.
 - [3] V.A. Kostelecký and S. Samuel, Phys. Rev. D **39**, 683 (1989); V.A. Kostelecký and R. Potting, Nucl. Phys. B **359**, 545 (1991).
 - [4] LSND Collaboration, A. Aguilar *et al.*, Phys. Rev. D **64**, 112007 (2001).
 - [5] MiniBooNE Collaboration, A.A. Aguilar-Arevalo *et al.*, Phys. Rev. Lett. **98**, 231801 (2007); Phys. Rev. Lett. **102**, 101802 (2009).
 - [6] MiniBooNE Collaboration, A.A. Aguilar-Arevalo *et al.*, Phys. Rev. Lett. **105**, 181801 (2010).
 - [7] MINOS Collaboration, P. Adamson *et al.*, arXiv:1104.0344.
 - [8] V.A. Kostelecký and M. Mewes, Phys. Rev. D **69**, 016005 (2004).
 - [9] J.S. Díaz and V.A. Kostelecký, Phys. Lett. B **700**, 25 (2011).
 - [10] V.A. Kostelecký and R. Potting, Phys. Rev. D **51**, 3923 (1995).
 - [11] O.W. Greenberg, Phys. Rev. Lett. **89**, 231602 (2002); arXiv:1105.0927.
 - [12] D. Colladay and V.A. Kostelecký, Phys. Rev. D **55**, 6760 (1997); Phys. Rev. D **58**, 116002 (1998).
 - [13] V.A. Kostelecký, Phys. Rev. D **69**, 105009 (2004).
 - [14] V.A. Kostelecký and N. Russell, Phys. Lett. B **693**, 2010 (2010); V.A. Kostelecký, Phys. Lett. B **701**, 137 (2011).
 - [15] *Data Tables for Lorentz and CPT Violation*, V.A. Kostelecký and N. Russell, Rev. Mod. Phys. **83**, 11 (2011).
 - [16] V.A. Kostelecký and M. Mewes, Phys. Rev. D **70**,

- 031902(R) (2004).
- [17] S. Choubey and S.F. King, Phys. Lett. B **586**, 353 (2004).
- [18] G. Lambiase, Phys. Rev. D **71**, 065005 (2005).
- [19] T. Katori *et al.*, Phys. Rev. D **74**, 105009 (2006).
- [20] V. Barger, D. Marfatia, and K. Whisnant, Phys. Lett. B **653**, 267 (2007).
- [21] N. Cipriano Ribeiro *et al.*, Phys. Rev. D **77**, 073007 (2008).
- [22] A.E. Bernardini and O. Bertolami, Phys. Rev. D **77**, 085032 (2008).
- [23] B. Altschul, J. Phys. Conf. Ser. **173** 012003 (2009).
- [24] S. Hollenberg, O. Micu, and H. Päs, Phys. Rev. D **80**, 053010 (2009).
- [25] S. Ando, M. Kamionkowski, and I. Mocioiu, Phys. Rev. D **80**, 123522 (2009).
- [26] M. Bustamante, A.M. Gago, and C. Peña-Garay, J. Phys. Conf. Ser. **171**, 012048 (2009).
- [27] S. Yang and B.-Q. Ma, Int. J. Mod. Phys. A **24**, 5861 (2009).
- [28] P. Arias and J. Gamboa, Int. J. Mod. Phys. A **25**, 277 (2010).
- [29] D.M. Mattingly *et al.*, JCAP **1002**, 007 (2010).
- [30] A. Bhattacharya *et al.*, JCAP **1009**, 009 (2010).
- [31] C.M. Ho, arXiv:1012.1053.
- [32] C. Liu, J.-t. Tian, and Z.-h. Zhao, Phys. Lett. B **702**, 154 (2011).
- [33] V. Barger, J. Liao, D. Marfatia, and K. Whisnant, arXiv:1106.6023.
- [34] V.A. Kostelecký and M. Mewes, Phys. Rev. D **70**, 076002 (2004).
- [35] J.S. Díaz *et al.*, Phys. Rev. D **80**, 076007 (2009).
- [36] LSND Collaboration, L.B. Auerbach *et al.*, Phys. Rev. D **72**, 076004 (2005).
- [37] M.D. Messier, in *CPT and Lorentz Symmetry III*, V.A. Kostelecký, ed., World Scientific, Singapore, 2005.
- [38] MINOS Collaboration, P. Adamson *et al.*, Phys. Rev. Lett. **101**, 151601 (2008).
- [39] MINOS Collaboration, P. Adamson *et al.*, Phys. Rev. Lett. **105**, 151601 (2010).
- [40] T. Katori, arXiv:1008.0906.
- [41] IceCube Collaboration, R. Abbasi *et al.*, Phys. Rev. D **82**, 112003 (2010).
- [42] V.A. Kostelecký, Phys. Rev. Lett. **80**, 1818 (1998).
- [43] KLOE Collaboration, A. Di Domenico, J. Phys. Conf. Ser. **171**, 012008 (2009); BaBar Collaboration, B. Aubert *et al.*, Phys. Rev. Lett. **100**, 131802 (2008); FOCUS Collaboration, J.M. Link *et al.*, Phys. Lett. B **556**, 7 (2003); KTeV Collaboration, H. Nguyen, hep-ex/0112046; V.A. Kostelecký, Phys. Rev. D **64**, 076001 (2001); Phys. Rev. D **61**, 016002 (2000).
- [44] D0 Collaboration, V.M. Abazov *et al.*, Phys. Rev. D **82**, 032001 (2010).
- [45] V.A. Kostelecký and R. Van Kooten, Phys. Rev. D **82**, 101702(R) (2010).
- [46] V.A. Kostelecký and M. Mewes, Phys. Rev. D **80**, 015020 (2009); in preparation.
- [47] Y. Nambu, Phys. Rev. Lett. **4**, 380 (1960); J. Goldstone, Nuov. Cim. **19**, 154 (1961); J. Goldstone, A. Salam, and S. Weinberg, Phys. Rev. **127**, 965 (1962).
- [48] V.A. Kostelecký and R. Potting, Gen. Rel. Grav. **37**, 1675 (2005); Phys. Rev. D **79**, 065018 (2009); S.M. Carroll, H. Tam, and I.K. Wehus, Phys. Rev. D **80**, 025020 (2009); J.L. Chkareuli, C.D. Froggatt, and H.B. Nielsen, Nucl. Phys. B **848**, 498 (2011).
- [49] V.A. Kostelecký and S. Samuel, Phys. Rev. D **40**, 1886 (1989); Phys. Rev. Lett. **63**, 224 (1989); R. Bluhm and V.A. Kostelecký, Phys. Rev. D **71**, 065008 (2005); R. Bluhm *et al.*, Phys. Rev. D **77**, 065020 (2008); O. Bertolami and J. Páramos, Phys. Rev. D **72**, 044001 (2005); M.D. Seifert, Phys. Rev. D **79**, 124012 (2009); Phys. Rev. D **81**, 065010 (2010); J. Alfaro and L.F. Urrutia, Phys. Rev. D **81**, 025007 (2010).
- [50] N. Arkani-Hamed, H.-C. Cheng, M. Luty, and J. Thaler, JHEP **0507**, 029 (2005); V.A. Kostelecký and J.D. Tasson, Phys. Rev. Lett. **102**, 010402 (2009); Phys. Rev. D **83**, 016013 (2011); B. Altschul *et al.*, Phys. Rev. D **81**, 065028 (2010).
- [51] P.F. Harrison, D.H. Perkins, and W.G. Scott, Phys. Lett. B **530**, 167 (2002).
- [52] Borexino Collaboration, G. Bellini *et al.*, Phys. Rev. D **82**, 033006 (2010).
- [53] KamLAND Collaboration, K. Eguchi *et al.*, Phys. Rev. Lett. **90**, 021802 (2003).
- [54] KamLAND Collaboration, T. Araki *et al.*, Phys. Rev. Lett. **94**, 081801 (2005); S. Abe *et al.*, Phys. Rev. Lett. **100**, 221803 (2008).
- [55] M. Gell-Mann, P. Ramond, and R. Slansky, in P. van Nieuwenhuizen and D.Z. Freedman, ed., *Supergravity*, North Holland, Amsterdam, 1979; T. Yanagida, in O. Sawada and A. Sugamoto, eds., *Workshop on Unified Theory and the Baryon Number of the Universe*, KEK, Japan, 1979; R. Mohapatra and G. Senjanović, Phys. Rev. Lett. **44**, 912 (1980).
- [56] For a review see, for example, P. Langacker, Int. J. Mod. Phys. A **18**, 4015 (2003).
- [57] MINOS Collaboration, P. Adamson *et al.*, Phys. Rev. Lett. **106**, 181801 (2011).
- [58] Super-Kamiokande Collaboration, Y. Ashie *et al.*, Phys. Rev. D **71**, 112005 (2005); Y. Fukuda *et al.*, Phys. Rev. Lett. **81**, 1562 (1998).
- [59] K2K Collaboration, M. H. Ahn *et al.*, Phys. Rev. Lett. **90**, 041801 (2003).
- [60] Super-Kamiokande Collaboration, Y. Ashie *et al.*, Phys. Rev. Lett. **93**, 101801 (2004).
- [61] R. Bluhm *et al.*, Phys. Rev. D **68**, 125008 (2003); Phys. Rev. Lett. **88**, 090801 (2002); V.A. Kostelecký and M. Mewes, Phys. Rev. D **66**, 056005 (2002).
- [62] Y. Declais *et al.*, Nucl. Phys. B **434**, 503 (1995).
- [63] M. Apollonio *et al.*, Eur. Phys. J. C **27**, 331 (2003).
- [64] G. Zacek *et al.*, Phys. Rev. D **34**, 2621 (1986).
- [65] F. Boehm *et al.*, Phys. Rev. D **64**, 112001 (2001).
- [66] L. Wolfenstein, Phys. Rev. D **17**, 2369 (1978); S. Mikheev and A. Smirnov, Sov. J. Nucl. Phys. **42**, 913 (1986); Sov. Phys. JETP **64**, 4 (1986); Nuovo Cimento **9C**, 17 (1986).
- [67] J.N. Bahcall, A.M. Serenelli, and S. Basu, Astrophys. J. Suppl. **165**, 400 (2006).
- [68] L. Borodovsky *et al.*, Phys. Rev. Lett. **68**, 274 (1992).
- [69] A. Romosan *et al.*, Phys. Rev. Lett. **78**, 2912 (1997); D. Naples *et al.*, Phys. Rev. D **59** 031101 (1999).
- [70] F. Dydak *et al.*, Phys. Lett. B **134**, 281 (1984).
- [71] CHORUS Collaboration, E. Eskut *et al.*, Phys. Lett. B **497**, 8 (2001).
- [72] NOMAD Collaboration, P. Astier *et al.*, Nucl. Phys. B **611**, 3 (2001).
- [73] NuTeV Collaboration, S. Avvakumov *et al.*, Phys. Rev. Lett. **89**, 011804 (2002).
- [74] MiniBooNE Collaboration, E.D. Zimmerman, talk at the 19th Particles and Nuclei International Conference, MIT,

Cambridge, Massachusetts, July 25, 2011.

- [75] V. Barger *et al.*, arXiv:0705.4396.
- [76] MINOS Collaboration, P. Adamson *et al.*, Phys. Rev. Lett. **103**, 261802 (2009); Phys. Rev. D **82**, 051102 (2010).
- [77] NO ν A Collaboration, D.S. Ayres *et al.*, arXiv:hep-ex/0503053.
- [78] T2K Collaboration, Y. Itow *et al.*, arXiv:hep-ex/0106019.
- [79] T2K Collaboration, C. Giganti, talk at the 2011 International Europhysics Conference on High Energy Physics, Grenoble, France, July 21, 2011.
- [80] Daya Bay Collaboration, X. Guo *et al.*, arXiv: hep-ex/0701029.
- [81] Double Chooz Collaboration, F. Ardellier *et al.*, arXiv: hep-ex/0606025.
- [82] RENO Collaboration, J.K. Ahn *et al.*, arXiv:1003.1391.
- [83] G. Mention *et al.*, Phys. Rev. D **83**, 073006 (2011).
- [84] J. Alonso *et al.*, arXiv:1006.0260.
- [85] OscSNS Collaboration, G.T. Garvey *et al.*, Phys. Rev. D **72**, 092001 (2005).